



1 Particle Inertia Effects on Radar Doppler Spectra Simulation

2 Zeen Zhu¹, Pavlos Kollias^{1,2} and Fan Yang¹

3 ¹Environmental and Climate Sciences Dept, Brookhaven National Laboratory, Upton, NY, USA

4 ² Division of Atmospheric Sciences, Stony Brook University, Stony Brook, NY, USA

5 *Correspondence to: Zeen Zhu (zzhu1@bnl.gov)*

6

7 **Abstract.** Radar Doppler spectra observations provide a wealth of information about cloud and
8 precipitation microphysics and dynamics. The interpretation of these measurements depends on
9 our ability to simulate these observations accurately forward. The effect of small-scale turbulence
10 on the radar Doppler spectra shape has been traditionally treated by implementing the convolution
11 process on the hydrometer reflectivity spectrum and environment turbulence. This approach
12 assumes that all the particles in the radar sampling volume respond the same to turbulent scale
13 velocity fluctuations and neglects the particle inertial effect. Here, we investigate the impact of
14 particle inertia on the forward modelled radar Doppler spectra. A physics-based simulation is
15 developed to demonstrate that big droplets, with large inertia, are unable to follow the rapid change
16 of velocity field in a turbulent environment. These findings are incorporated to a new radar Doppler
17 spectra simulator. Comparison between the traditional and the newly formulated radar Doppler
18 spectra simulators indicates that the conventional simulator leads to an unrealistic broadening of
19 the spectrum, especially in strong turbulence environment. Doppler spectra observed from the W-
20 band Cloud Radar at South Great Plain (SGP) observatory are used to validate the fidelity of the
21 two Doppler spectrum simulation methods. The result indicates that the Doppler spectrum
22 generated from the proposed approach is more consistent to the observed Doppler spectrum while
23 the conventional simulator misrepresents the Doppler spectrum morphology. This study provides
24 clear evidence to illustrate the droplets inertial effect on radar Doppler spectrum and develops a
25 physics-based simulator framework to accurately emulate the Doppler spectrum for a given
26 Droplet Size Distribution in turbulence field. The proposed simulator has various potential
27 applications to the cloud/precipitation studies and provides a valuable tool to decode the cloud
28 microphysics and dynamics properties from Doppler radar observation.

29

30

31



32 **1 Introduction**

33 The radar Doppler spectrum represents the frequency (velocity) distribution of the
34 backscattered radar signal at a particular range. In a vertically pointing radar, the Doppler spectra
35 provides the distribution of the backscattered signal over a range of Doppler velocities, whose
36 value depends on the dynamical (i.e., vertical air motion) and cloud microphysical (i.e.,
37 hydrometeors concentration and sizes) properties within the radar sampling volume. A variety of
38 research applications that utilize the full radar Doppler spectrum have been developed. For
39 instance, Doppler spectrum can be used to resolve rain Droplet Size Distribution (DSD) (Atlas et
40 al., 1973), remove clutters and identify hydrometers signals (Williams et al., 2018; Luke et al.,
41 2008; Moisseev and Chandrasekar, 2009), identify drizzle development stage (Zhu et al.,
42 2022; Acquistapace et al., 2019), retrieve vertical air motion (Kollias et al., 2002; Williams,
43 2012; Zhu et al., 2021), characterize the melting-layer properties (Li and Moisseev, 2020; Mróz et
44 al., 2021), and to validate and improve the microphysical modeling process (Kollias et al., 2011b).
45 Combined with the depolarization capability, Doppler spectrum can also be used for cloud-phase
46 classifications and to investigate ice-cloud microphysical process (Luke et al., 2010; Luke et al.,
47 2021; Kalesse et al., 2016; Oue et al., 2018). The list of widely application of the Doppler spectrum
48 in the cloud-precipitation research mentioned above is by no means exhaustive.

49 Even though the significance of radar Doppler spectrum is highly recognized, spectrum
50 itself is challenging to be unambiguously interpreted to characterize the cloud/precipitation
51 properties. One important reason is a lack of fully understanding of the entanglement between the
52 hydrometer microphysics and environment dynamics as well as their manifestation on the Doppler
53 spectrum morphology (Kollias et al., 2002). More specifically, Doppler spectrum is contributed
54 by hydrometer DSD, vertical air motion and environment turbulence: the width of Doppler
55 spectrum is contributed by both DSD and small-scale turbulence, while the Doppler frequency
56 shift is a combined measure of the air motion and the particles falling velocity (Doviak, 2006). A
57 successful separation of the microphysical and dynamical contributions to Doppler spectrum is
58 essential to reduce the retrieval uncertainties and to better characterize the cloud-precipitation
59 properties (Zhu et al., 2021).

60 Radar Doppler spectra simulators have been invaluable for the interpretation of the radar
61 Doppler spectra shape (Capsoni et al., 2001; Oue et al., 2020; Kollias et al., 2011a; Maahn et al.,
62 2015). Traditionally, the impact of turbulence on the shape of the radar Doppler spectrum is



63 represented by the convolution of the quiet air (no air motion) power spectrum with a Gaussian
64 distribution (Gossard and Strauch, 1989). The width of the Gaussian distribution is parameterized
65 as a function of the radar parameters and the turbulence intensity often represented in terms of
66 eddy dissipation rate (Borque et al., 2016). This approach is only valid under the assumption that
67 the droplet inertia effect is negligible and droplets with different sizes can follow exactly the
68 environment wind field. In reality, however, big droplets with large inertia cannot follow the rapid
69 change of wind velocity field as the small droplets perform (Yanovsky, 1996;Lhermitte, 2002).
70 Not accounting for the particle inertia effect can lead to a misinterpretation of the Doppler
71 spectrum and cause large uncertainties for the retrieval product (Nijhuis et al., 2016).

72 Several physics-based frameworks have been proposed to simulate the droplet motions in
73 turbulence (Khvorostyanov and Curry, 2005;Lhermitte, 2002). Here, the approach proposed by
74 Lhermitte (2002) is used to illustrate the droplets inertial effect and to investigate this effect on the
75 radar Doppler spectrum. In detail, we aim to answer the following questions: 1) How inertia affect
76 the response of a droplet in a fluctuating turbulent wind field? 2) Is this effect significant on
77 simulated and observed radar Doppler spectra? and 3) How can we account for the droplet inertia
78 in radar Doppler spectra simulators? Building on these investigations, a new approach to generate
79 radar Doppler spectra is described.

80 The structure of this paper is organized as follows: section 2 introduces the observational
81 dataset used in this study; section 3 describes the physical modeling framework used to simulate
82 the droplet movement and to illustrate the droplets inertia effect in a turbulent environment; section
83 4 proposes the physics-based Doppler spectrum simulator and compares the emulated spectra to
84 the ones generated from the traditional method; section 5 uses real observed Doppler spectra to
85 validate the fidelity of the proposed spectrum simulator; section 6 concludes the major results of
86 this study and followed by a discussion.

87

88

89 **2 Data**

90 The dataset used in this study are collected at the U.S. Department of Energy Atmospheric
91 Radiation Measurement (ARM) Southern Great Plain (SGP) observatory at Lamont, OK. The
92 primary instrument being used is the W-band ARM Cloud Radar (WACR). WACR is a vertical
93 pointing radar operating at 95.04 GHz with a range resolution of 42.8 m and a temporal resolution



94 of 4.28 s. Since 2005, WACR has been continuously collecting Doppler spectra with 256 Doppler
95 velocity bins and with a Nyquist velocity of $\pm 7.8 \text{ ms}^{-1}$. (Kollias et al., 2016). Doppler spectra post-
96 processing algorithm (Hildebrand and Sekhon, 1974) is implemented to remove noise and identify
97 the hydrometer signals. In addition, impact disdrometer which records the DSD of raindrops is
98 used to evaluate the radar Doppler spectrum near surface. Disdrometer measures rain drop size
99 over the range from 0.3 mm to 5.4 mm categorized by 20 diameter bins with a time resolution of 1
100 minute (Wang et al., 2021). The specified accuracy of drop size measurement is estimated as $\pm 5\%$.

101

102 **3 Simulation of raindrops movement in turbulence environment**

103 In this section, a physics-based simulation framework to illustrate the droplets inertia effect
104 in given turbulence environment is presented. First, we will introduce the equations being used to
105 describe droplets movement according to Lhermitte (2002). Then a generated turbulent wind field
106 is applied to resolve the droplets velocity and to discuss the implication of inertia effect on the
107 simulated Doppler spectrum.

108

109 **3.1 Motion of droplets in a turbulent environment**

110 Assuming a liquid droplet with a diameter of D , the motion of the droplet can be described as:

111

$$112 \quad F = m \frac{dV_D}{dt} \quad (1)$$

113

114 where m is the droplet mass, V_D is the droplet velocity, F is the drag force exerted by wind
115 expressed as:

116

$$117 \quad F = \frac{C_d S (V_w - V_D)^2 \rho_a}{2} \quad (2)$$

118 where C_d is the wind drag coefficient, V_w is wind velocity, ρ_a is air density, S is the droplet cross
119 section normal to wind direction. For spherical droplets, S can be calculated as:

120

$$121 \quad S = \frac{\pi D^2}{4} \quad (3)$$

122



123 and droplet mass (m) is calculated as:

124

$$125 \quad m = \frac{1}{6} \pi \rho_l D^3 \quad (4)$$

126

127 where ρ_l is liquid water density. Finally, wind drag coefficient C_d is obtained from an
128 experimental fitted function adapted from (Lhermitte, 2002)

129

$$130 \quad \log C_d = 1.445 - 0.8796 \times \log Re + 0.0642 \times (\log Re)^2 + 0.0104 \times (\log Re)^3 \quad (5)$$

131

132 where Re is the Reynolds number estimated as:

133

$$134 \quad Re = \frac{(V_w - V_D) D \rho_a}{\mu} \quad (6)$$

135

136 where μ is the air dynamic viscosity. Here, ρ_a , ρ_l , and μ are used as 1.22 kg m^{-3} ,
137 1000 kg m^{-3} , $1.81 \times 10^{-5} \text{ kg m}^{-1} \text{ s}^{-1}$ as a representation of environment with 15°C and 1000
138 hPa .

139 Combining (1)-(6), the droplet velocity (V_D) as a function of time can be calculated numerically
140 if the wind field (V_w) is given.

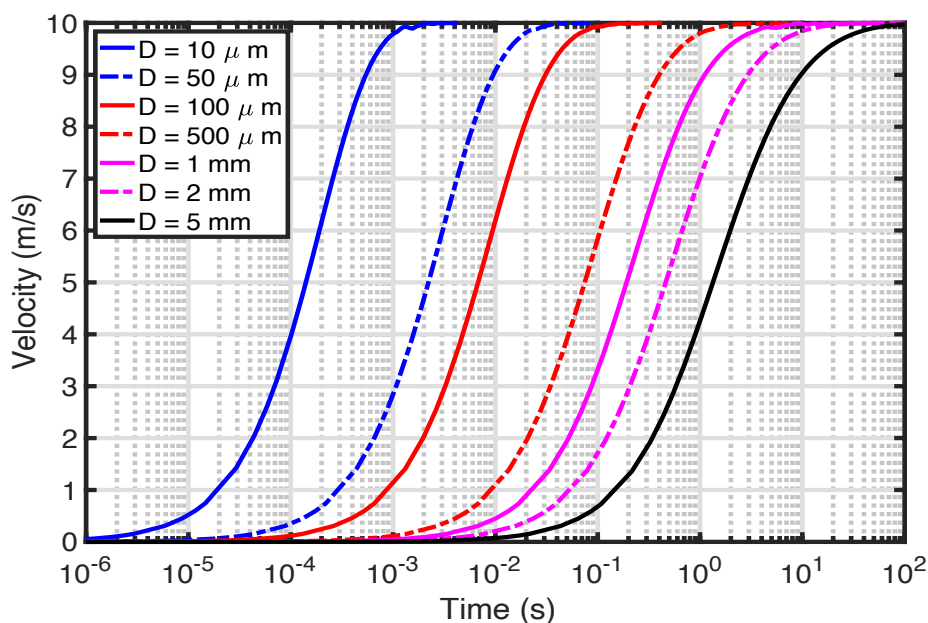
141

142 **3.2 Illustration of droplet inertial effect**

143 We first illustrate the inertial effect by calculating droplets motion under a constant wind
144 velocity field. Seven droplets with diameters of $10 \mu\text{m}$, $50 \mu\text{m}$, $100 \mu\text{m}$, $500 \mu\text{m}$, 1 mm , 2 mm , 5
145 mm are selected to cover the size range of cloud, drizzle and raindrops. Initial velocity of all the
146 droplets is 0 ms^{-1} , a constant wind velocity with 10 ms^{-1} is exerted upon the droplets when $t > 0 \text{ s}$.
147 Due to the drag force, droplets start to move but with different accelerations depending on droplet
148 inertia: droplets with small inertia are accelerated more quickly than larger ones. This effect is
149 clearly illustrated in Figure 1: droplet with diameter of $10 \mu\text{m}$ quickly reach to the wind velocity
150 within only 0.002s , while droplets with 1 mm and 5 mm need 5 and 50s respectively to adjust
151 their motion to the exerted wind velocity. The different response time of droplets with different



152 sizes to the exerted wind velocity suggests that small droplets are more capable to follow the
153 velocity variation than their large counterparts.
154

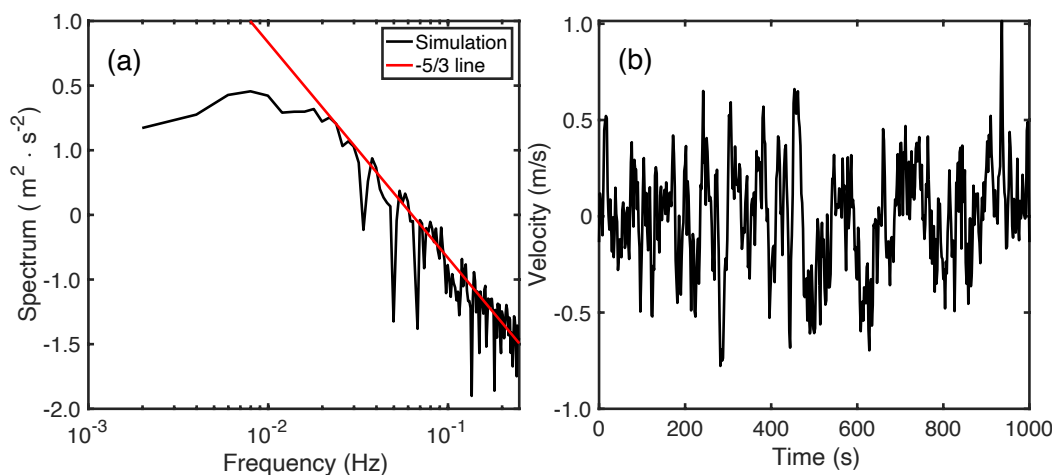


155 Figure 1. Velocity of droplets with diameter of $10 \mu\text{m}$ (blue solid line), $50 \mu\text{m}$ (blue dash-dot line),
156 $100 \mu\text{m}$ (red line), $500 \mu\text{m}$ (red dash-dot line), 1 mm (magenta solid line), 2 mm (magenta dash-
157 dot line) and 5 mm (black solid line) as function of time after exerted by a constant wind with 10
158 ms^{-1} velocity.

159 In real atmosphere, air velocity is not constant but fluctuates with time as a representative
160 of turbulent nature. In order to emulate the turbulence environment, a 1-D turbulence field is
161 generated with 2 Hz sampling frequency, 1000s duration and with a standard deviation of 0.3 ms^{-1}
162 ¹ using the method proposed by Deodatis (1996). The selection of 0.3 ms^{-1} standard deviation is
163 based on a quantitatively estimation of cloud radar observation under a typical stratiform
164 environment (Zhu et al., 2022). Specifically, for cloudy condition with an eddy dissipation rate
165 (EDR) of $1 \times 10^{-3} \text{ m}^2 \text{ s}^{-3}$, Doppler spectrum width observed from radar with 30m range resolution
166 and 0.3° beamwidth at 1km height is estimated to be 0.27 ms^{-1} (Borque et al., 2016). The spectrum
167 and time series of the generated air velocity are shown in Figure 2: the turbulence spectrum (Figure
168 2a) characterizes typical inertial subrange of the turbulence scale with a standard deviation of 0.3
169 ms^{-1} (Figure 2b).



170



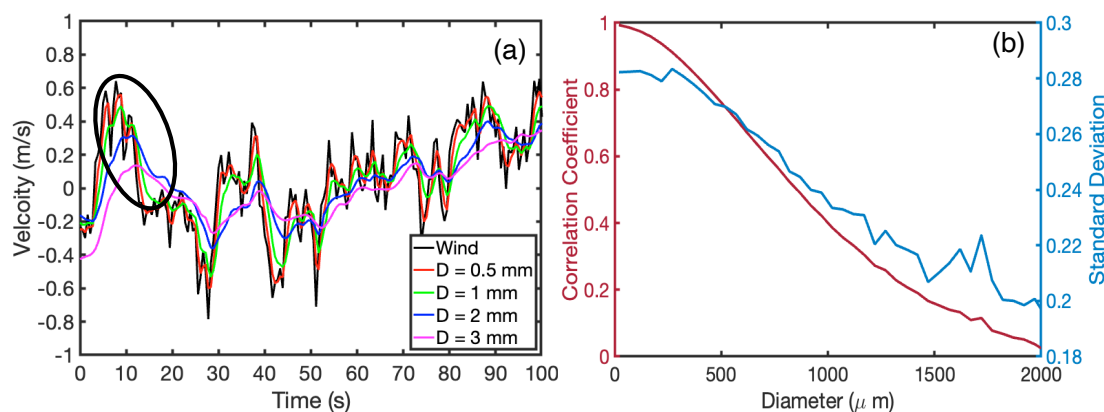
171 Figure 2. (a) Spectrum of the simulated turbulence (black line), red line represents the -5/3 slope.
172 (b): Time series of vertical velocity for the simulated turbulence.

173

174 The generated air velocity is assigned to V_w (Eq. (2)) to simulate the motion of droplets.
175 Figure 3a shows the time-dependent velocity of droplets with selected diameter of 0.5 mm, 1 mm,
176 2 mm, 3 mm. Droplets with different sizes response differently with the change of wind velocity,
177 and there are two notable characteristics due to the inertial effect (highlighted in the black oval in
178 Fig. 3a). First, large droplets need longer time to adjust to the wind velocity, and thus there is a
179 distinct time-lag when the peak velocity is reached for different particles. Second, in addition to
180 the time-lag, the peak velocity reached by the large droplets is smaller than the small droplets.
181 Here, we use correlation coefficient between the actual wind velocity and the droplet velocity to
182 quantify the inertial effect. A correlation coefficient of 1 represents droplets can follow exactly the
183 wind velocity and a correlation coefficient less than 1 indicates a time-lag effect between the wind
184 and droplet velocity due to droplet inertia. Figure 3b shows that the correlation coefficient is close
185 to 1 when the droplets are smaller than 50 μm but it decreases dramatically as droplet size increases.
186 The correlation coefficient reaches to 0 when diameter reaches to 2000 μm . In addition, for
187 droplets with diameters smaller than 300 μm the standard deviation of the actual droplet velocity
188 is 0.29 ms^{-1} (blue curve, Figure 3b), which is closely to standard deviation of the background wind
189 field. As droplet size increases, the velocity variation decreases due to droplet inertial effect.



190 The simulation results shown in Figure 3 suggest that small droplets are equivalently
191 inertia-free and can instantaneously adjust their velocity to that of the imposing wind field, and
192 thus, small cloud droplets can be treated as perfect air tracers (Kollias et al., 2001). On the other
193 hand, large droplets ($D > 0.5$ mm) exhibit a time lag in their response to the air motion and an
194 amplitude reduction (inertial-based filtering). As the observed Doppler velocity is a combined
195 measure of the droplet velocity and the ambient air motion, this droplet inertial effect is expected
196 to have a considerable effect on the generated radar Doppler spectrum. In the following section,
197 we will illustrate how the radar Doppler spectrum is affected by droplet inertia and how to account
198 for this effect in radar Doppler spectrum simulations.



199 Figure 3. (a) Generated wind velocity filed (black line) and the resolved velocity for particles with
200 diameter of 0.5mm (red line), 1mm (green line), 2mm (blue line) and 3mm (magenta line). The
201 black oval indicates the period showing clear droplet inertia effect. (b) Left axis: correlation
202 coefficient between wind filed and droplet velocity for different droplets size; right axis: standard
203 deviation of the droplets velocity with different droplets size. Only droplets with size from $0\ \mu\text{m}$
204 to $2000\ \mu\text{m}$ are shown for the sake of clarity.

205

206 4 Radar Doppler spectrum Simulator

207 Two methodologies for simulating the radar Doppler spectrum for a given DSD and
208 turbulence conditions are used here. The first approach is the traditional one. All droplets,
209 independent of their sizes, are assumed to have no inertial effects and thus act like perfect tracers.
210 In this case, the effect of turbulence is represented through the convolution of a Gaussian
211 distribution determined by EDR and the radar specifications with the quiet air radar Doppler



212 spectrum depending on cloud droplet size distribution(Gossard, 1981; Kollias et al., 2011, Zhu et
213 al., 2021). A brief overview of the traditional method is described in section 4.1.

214 The second approach is based on the physics-based simulation described in Section 3.1
215 which will resolve the exact droplets velocity at each specific time. The time step of the simulation
216 is set as 0.05s to accommodate the typical ARM cloud radar setting with approximately 40 spectra
217 being averaged in 2s. The corresponding Doppler spectrum at each timestep is estimated and the
218 final Doppler spectrum is obtained by averaging the spectra over the simulation duration. The
219 second method is designed to capture the inertia effect of the droplets and it can be used as a
220 benchmark to validate the Doppler spectrum generated from the traditional way. It is noted that
221 the Doppler spectrum simulator discussed in this study is only applied to the vertical pointing
222 radars.

223

224 4.1 Traditional Doppler spectrum simulator

225 For a given DSD described by a number concentration $N(D)$ per unit of volume in m^{-4} , the
226 radar reflectivity $d\eta(D)$ (m^2/m^3) from particles with diameter between D to $D + dD$ can be
227 expressed as:

$$228 \quad d\eta(D) = N(D)\sigma_b(D)dD \quad (7)$$

229 where $\sigma_b(D)$ is the backscatter cross section (m^2) of a particle with diameter D in m. Mie scattering
230 theory is used to estimate $\sigma_b(D)$. In this formulation, the radar power spectrum distribution is
231 provided in terms of particle size. Profiling radar do not observe the radar backscatter-energy
232 power spectrum $d\eta(D)$ but the radar Doppler spectra density $S_q(V_t)$ where V_t in the droplet fall
233 velocity in ms^{-1} . The conversion from droplet size to droplet fall velocity requires a $V_t(D)$
234 relationship. Here, the expression proposed by (Lhermitte, 2002) is used to relate the droplets fall
235 velocity (V_t) as a function of diameter (D):

236

$$237 \quad V_t(D) = 920 \times (1 - \exp(-6.8 \times D^2 - 4.88 \times D)) \quad (8)$$

238

239 where the unit of D and V_t is in cm and cms^{-1} respectively. Subsequently, the radar Doppler
240 spectral density $S_q(V_t)$ in units of $m^2m^{-3}/(ms^{-1})$ is given by:

$$241 \quad S_q(V_t) = \frac{d\eta}{dV_t} = \frac{d\eta}{dD} \frac{dD}{dV_t} = N(D)\sigma_b(D) \frac{dD}{dV_t} \quad (9)$$



242 where $\frac{dD}{dv_t}$ is estimated from Eq. 8.

243 The $S_q(V_t)$ is the “quite-air” radar Doppler spectrum where the only velocity contribution
244 is the droplet fall velocity. In the real atmosphere, the observed velocities from the radar include
245 the turbulent motions with scales larger or smaller than that of the radar sampling volume (Kollias
246 et al., 2001; Borque et al., 2016). One parameter that is typically used to describe turbulence
247 intensity is the eddy dissipation rate (EDR in m^2s^{-3}). The EDR value can be converted to a radar
248 Doppler spectrum broadening term σ_t in ms^{-1} (Borque et al., 2016). It is important to note that the
249 σ_t value strongly depend on the radar sampling characteristics (Kollias et al., 2005). For the same
250 EDR value, σ_t is lower for radar systems with short time dwell, narrow beamwidth and short pulse
251 length (Borque et al., 2016). The σ_t is typically used to introduce the effect of turbulence on the
252 radar Doppler spectrum. Under the assumption of isotropic turbulence, the distribution of the
253 turbulent motions within the radar sampling volume can be approximated using a Gaussian
254 function (Gossard and Strauch, 1989):

$$255 \quad G(v) = \frac{1}{\sigma_t \sqrt{2\pi}} \times \exp\left(-\frac{1}{2} \left(\frac{v}{\sigma_t}\right)^2\right) \quad (10)$$

256 And its impact on the radar Doppler spectra is formulated using the convolution of $S_q(V_t)$ and
257 $G(v)$ as:

$$258 \quad S(v) = (S_q * G)(v) = \int_{-\infty}^{\infty} S_q(u) G(v - u) du \quad (11)$$

259

260 **4.2 Physics-simulation based Doppler spectrum simulator**

261 In this approach, instead of using a Gaussian distribution to parameterize turbulence field
262 and applying the convolution process to represent the interaction between DSD and environmental
263 turbulence, the radar Doppler spectrum generation is based on a large number of real droplet
264 velocity simulations for a given turbulence intensity. Droplet velocity of each diameter at each
265 given time ($V(D, t)$) is resolved in the entire simulated time domain based on the equations
266 described in Section 3.1. At each time step, the DSD Doppler spectrum is simulated similar as Eq
267 9:

$$268 \quad S_t(V_t) = N(D) \sigma_b(D) \frac{dD}{dV_t} \quad (12)$$

269



270 Here $\frac{dD}{dv_t}$ is obtained from the resolved $V(D, t)$.

271 The final Doppler spectrum is obtained by averaging all the DSD Doppler spectra (S_t) at each
272 timestep:

$$273 \quad S(v) = \frac{1}{N_t} \sum_{n=1}^{n=N_t} S_t \quad (13)$$

274 where N_t is the total simulation timesteps:

$$275 \quad N_t = T \times f$$

276 Where T and f is the time duration and the sampling frequency for the generated turbulence
277 wind field.

278
279

280 **4.3 Doppler spectra comparison from two simulators**

281 Both simulators described above are applied to emulate the Doppler spectrum observed by
282 a 94-GHz (W-band) profiling cloud radar for a given DSD and for a set of different turbulence
283 environments. The W-band radar parameter settings are similar with of the W-band ARM Cloud
284 Radar (WACR) operated at the ARM observatory at the SGP site. The Nyquist velocity is set at \pm
285 6 ms^{-1} and a 256-point Fast Fourier Transform (FFT) is used to represent the WACR Doppler
286 spectrum. The Marshall-Palmer exponential DSD (Marshall and Palmer, 1948) with
287 $N(D) = N_0 e^{-\Lambda D}$ is used to represent the DSD in the WACR sampling volume. N_0 is intercept
288 parameter of 0.08 cm^{-4} and Λ is slope factor of 15 cm^{-1} , droplets diameter ranges from 10 to 4000
289 μm with bin size as $1 \mu\text{m}$. Turbulence field is generated with 20 Hz frequency (f), 100s duration
290 (T) and standard deviation (σ) with 0.05 ms^{-1} , 0.25 ms^{-1} , 0.35 ms^{-1} and 0.45 ms^{-1} , respectively. The
291 reason of applying different turbulence settings is to better illustrate the droplet inertia effect under
292 different turbulence environment. It is expected that with increasing turbulence intensity the
293 droplet inertia effect will be manifested in larger differences for the generated radar Doppler
294 spectrum from two methods. The selection of W-band radar and the use of a rain DSD is because
295 it is well known that due to non-Rayleigh scattering, the W-band radar Doppler spectra in rain
296 contains oscillations that can be used to pinpoint the differences between the two methodologies
297 for simulating the radar Doppler spectrum (Kollias et al., 2002; Kollias et al., 2007). For the



298 proposed simulation approach, an adjusted time is required for droplets reaching to steady state,
299 after which the droplets of different size fluctuate near terminal velocity with variations induced
300 by the forced wind. The adjusted time for the aforementioned setting is around 20s but may vary
301 according to the wind field and droplets size being applied. To generate a smooth Doppler spectra
302 and to avoid the updraft/downdraft trend in a relatively short period, sufficient number of simulated
303 spectra needed to be averaged. Here the simulated spectra are averaged over 50s, this time is longer
304 than the ARM cloud radar dwell time, but is a valid consideration under the assumption that
305 turbulence is homogenous over time.

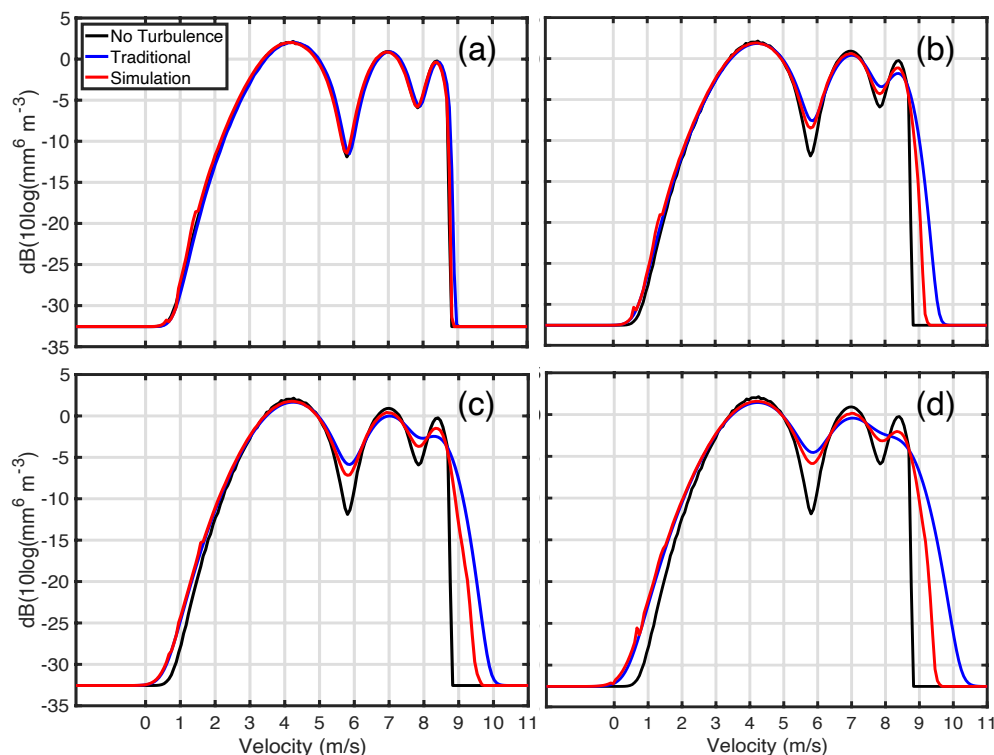
306 The results shown in Figure 4 echoes the expectation. In a turbulence environment with σ_t
307 as 0.05 ms^{-1} (Figure 4a), the two simulated spectra (red and blue line in Figure 4a) and the
308 simulated Doppler spectrum without turbulence broadening (black line) are almost overlapping
309 with each other, indicating that the radar Doppler spectrum shape is dominated by the DSD shape
310 and the droplets fall velocity in weak turbulence conditions. For σ_t equal to 0.25 ms^{-1} , the
311 broadening of the right edge of the radar Doppler spectrum in the physics-simulation approach
312 (red line in Figure 4b) is less than that produced with the convolution approach (blue line in Figure
313 4b). As σ_t increases to 0.35 ms^{-1} , the large difference right edges of the spectrum from two
314 simulators are clearly identified. Moreover, the two non-Rayleigh scattering resonant notches in
315 the radar Doppler spectrum (Kollias et al., 2002) also exhibit considerable differences. In addition,
316 the convoluted Doppler spectrum (obtained from the traditional method, blue line in Figure 4c)
317 that ignore droplet inertial effect fills more the scattering valley, while the simulated spectrum
318 (obtained from the physics-simulation approach) results to less velocity spread and thus, less filling
319 of the scattering minima (red line in Figure 4c). In particular, the second notch around 8 ms^{-1} from
320 the convoluted spectrum begins to fill up, while it is still clearly identified for the simulated
321 spectrum; when σ_t reaches to 0.45 ms^{-1} , the right edge velocity difference between two spectra is
322 larger than 1 ms^{-1} , and the second notch on the convoluted spectrum (blue line in Figure 4d)
323 completely disappears, while is still recognizable on the simulated spectrum (red line in Figure 4d).
324 The first notch of the simulated spectrum is also deeper than that from the traditional method.
325 Another notable finding is the left part of Doppler spectra (velocity smaller than 4 ms^{-1}) from two
326 simulators almost overlap with each other in different turbulence scenarios, as this part of the
327 spectrum is mostly contributed by small droplets with negligible inertial effect, and the



328 corresponding Doppler spectrum can be correctly represented by the traditional convolution
329 process.

330 Compared with the three generated Doppler spectra in Figure 4, we can clearly identify the
331 effect of droplet inertia on Doppler spectrum morphology under different turbulence environments.
332 In general, both two simulators indicate a wider Doppler spectrum under a large turbulence
333 condition, but with different broadening magnitudes. The traditional approach generates a wider
334 spectra and a larger notch power in a more turbulent environment. This overestimation of the
335 turbulence broadening effect indicates that the convolution process used in the conventional
336 simulator is unable to accurately represent the interaction between DSD and turbulence field. On
337 the other hand, for the small droplets, the inertial effect is negligible and the generated Doppler
338 spectra are consistent from two approaches. It is therefore concluded that the convolution process
339 can simulate the Doppler spectrum for the light drizzle precipitation which mostly occurs in marine
340 boundary layer clouds but it is inadequate to emulate Doppler spectrum for the heavy precipitation
341 in deep convection, especially in the presence of strong turbulence environment.

342





343 Figure 4. Doppler spectra generated by traditional (blue line) and simulated (red line) approach for
344 turbulence with (a) 0.05 ms^{-1} , (b) 0.25 ms^{-1} , (c) 0.35 ms^{-1} , (d) 0.45 ms^{-1} . Black line represents
345 generated Doppler spectrum without turbulence ($\sigma_t = 0$).

346

347

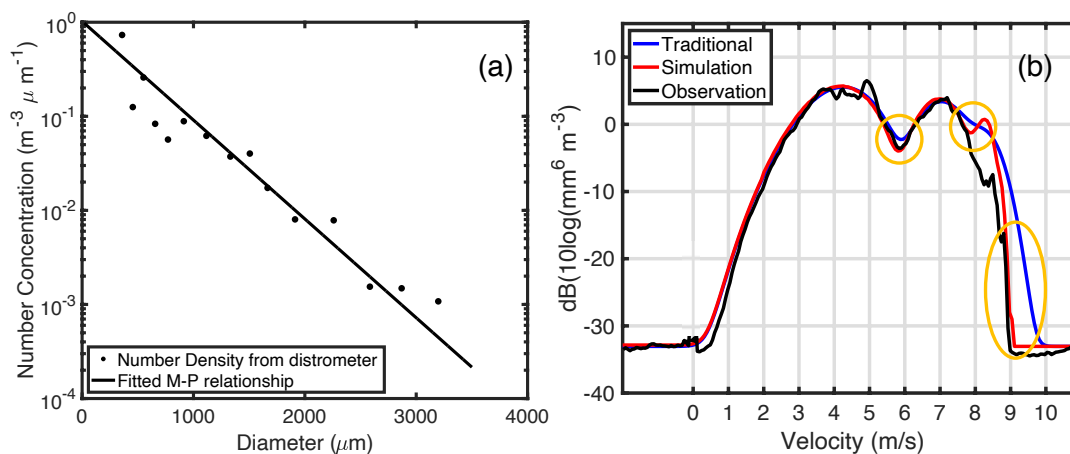
348 **5 Doppler spectra comparison with observation**

349 Here, we use the WACR-observed Doppler spectrum during a heavy precipitation event to
350 evaluate the two methodologies for simulating the W-band radar Doppler spectra in rain. The
351 WACR observations were collected at the ARM SGP site on May 9, 2007. The rain DSD observed
352 at the surface from a disdrometer is shown in Figure 5a. An exponential fit is applied to the
353 recorded DSD to extract the Marshal-Palmer parameters that best capture the observed rain DSD
354 (black line in Figure 5a). The WACR Doppler spectra at the lowest radar range gate (460m) are
355 collected during the same period from 05:44 to 05:45 UTC coinciding with disdrometer
356 observation. The turbulence parameter (σ_t) is calculated using the approach proposed by Borque
357 et al. (2016) with average σ_t as 0.33 ms^{-1} . Based on the fitted DSD and retrieved σ_t , the simulated
358 radar Doppler spectra from the traditional method (blue line) and from the physics-simulation
359 method (red line) are estimated (Figure 5b).

360 The left part of the radar Doppler spectrum from the two simulators are similar and
361 consistent to the observations. This is expected since the left part of the radar Doppler spectrum is
362 occupied by small droplets and the droplet inertia is expected to be negligible. At the right part of
363 the radar Doppler spectrum, three noticeable differences are identified (highlighted in the yellow
364 oval). First, the right edge of the spectrum from the simulation-approach is consistent with the
365 observed spectrum while the traditional approach generates a much wider spectrum. Second, the
366 first notch (around 6 ms^{-1}) of the simulated spectrum overlaps with the observed spectrum very
367 well while the first notch from the traditional approach has larger spectral power related to the
368 observation. Finally, the second notch (around 8 ms^{-1}) in the simulated spectrum is distinguishable,
369 while it completely disappears from the spectrum generated by traditional approach. It is noted,
370 however, that both the simulated Doppler spectra near the second notch is not consistent with the
371 real observation, these inconsistencies may be attributed to the fact that the fitted Marshal-Palmer
372 relationship is not an adequate representation of the DSD observed from WACR.



373 The spectra comparison shown in Figure 5 provides supporting evidence that the proposed
374 physics-simulation approach can generate a more realistic Doppler spectrum as observed from real
375 radar observation. Compared with the conventional approach, the proposed simulator has
376 significant improvement to correctly emulate the turbulence broadening on Doppler spectrum due
377 to the inertia effect of large droplets. This improved simulator provides a valuable tool to interpret
378 the radar observation and to decode the precipitation DSD and environmental dynamics
379 information contained in the Doppler spectrum.



380
381 Figure 5. (a) Dots represent the observed raindrop number concentration from disdrometer at 05:44
382 (UTC) on May 9, 2007 on SGP site, black line represents the fitted Marshall-Palmer relationship
383 with slope (Λ) of 24 and intercept (N_0) of 0.01 cm^{-4} . (b) Doppler spectra generated from simulation
384 (red) and traditional (blue) method. Black line is the observed spectrum from WACR.

385

386 6 Conclusions

387 The radar Doppler spectra offer unprecedented capabilities for studying cloud and
388 precipitation microphysics. Recent advancements in radar technology and signal processing have
389 enable the continuous recording of high-quality radar Doppler spectra observations from a wide
390 range of profiling radar systems (Kollias et al., 2005; Kollias et al., 2016). Until now, the simulation
391 of the radar Doppler spectra was based on well-established techniques (Gossard, 1988; Kollias et
392 al., 2011a). However, inertial effect of large droplets is constantly being neglected in the design of
393 current simulators. Here, the impact of the droplet's inertia in the representation of atmospheric



394 turbulence on the shape of the radar Doppler spectrum was investigated. A physics-based
395 simulation framework is developed to resolve the droplets velocity in a given turbulence
396 environment. It demonstrates that big droplets with large inertia will take longer time to adapt to
397 the change of velocity field, indicating large droplets are incapable to follow the turbulence wind
398 as small droplets behave.

399 Building on the simulation framework, a new approach is proposed to emulate Doppler
400 spectrum by resolving the velocity of each droplet during the entire time domain. The simulated
401 W-band radar Doppler spectrum is compared with the one generated from the traditional method
402 for a typical DSD with four different turbulence environments. The comparison indicates that the
403 traditional Doppler simulator without considering the inertial effect generates an artificially
404 broader spectrum and a misrepresentation of the spectrum notch power. This inertia effect becomes
405 more noticeable as turbulence intensity increases. This finding suggests that special caution should
406 be taken for the applicability of using convolution process to represent DSD-turbulence interaction
407 in heavy precipitation. In the case of light precipitation mostly happening in marine boundary layer
408 cloud, the droplet inertia effect on Doppler spectrum is negligible and the traditional simulator
409 generates consistent results with the proposed simulator.

410 The WACR Doppler spectra collected from the SGP observatory are compared with the
411 simulated spectra to testify the fidelity of the two simulators. The results show that the proposed
412 physics-simulation approach has a better representation of the observed Doppler spectra
413 morphology compared with the traditional simulator. The convolution process used in the
414 conventional simulator fails to consider the large droplet inertia effect thus results in an
415 overestimation of the turbulence broadening effect and a broader Doppler spectrum.

416 An accurate simulation of the Doppler spectrum is essential to improve the fundamental
417 understanding of radar observation. The proposed Doppler spectrum simulator, with the ability to
418 resolve the individual droplet movement, can emulate a more realistic Doppler spectrum and
419 provide various of potential applications to the research community. For instance, neglecting
420 droplet inertia effect on radar Doppler spectrum increases the retrieval uncertainty of the eddy
421 dissipation rate (Nijhuis et al., 2016). This simulator can quantitatively estimate the inertia effect
422 and improve the retrieval accuracy. The forward Doppler spectra simulator can also be utilized to
423 connect radar observation and modeling output to evaluate the model performance (Oue et al.,
424 2020; Mech et al., 2020; Silber et al., 2022). We expect this proposed Doppler spectrum simulation



425 framework can stimulate more studies to better interpret the Doppler radar observation and to
426 advance the understanding of the microphysics and dynamics information concealed in radar
427 Doppler spectrum.

428

429 **Competing interests.**

430 **P. K.** is the associate editor of AMT and the peer-review process was handled by an independent
431 editor. The authors have no other competing interests to declare.

432

433 **Code/Data availability**

434 Ground-based data were obtained from the Atmospheric radiation measurement (ARM) user
435 facility, a U.S. Department of Energy (DOE) Office of Science user facility managed by the Office
436 of Biological and Environment Research.

437 W-Band (95 GHz) ARM Cloud Radar (WACRSPECCMASKCOPOL). 2007-05-09 to 2007-05-
438 10, Southern Great Plains (SGP) Central Facility, Lamont, OK (C1). Compiled by K. Johnson, D.
439 Nelson and A. Matthews. ARM Data Center. Data set accessed 2022-07-
440 05 at <http://dx.doi.org/10.5439/1025318>.

441 Impact Disdrometer (DISDROMETER). 2007-05-09 to 2007-05-10, Southern Great Plains
442 (SGP) Central Facility, Lamont, OK (C1). Compiled by D. Wang. ARM Data Center. Data set
443 accessed 2022-07-05 at <http://dx.doi.org/10.5439/1025181>.

444

445 The codes being used in this study (section 3.2) to generate the turbulence field can be accessed
446 from (https://github.com/ECheynet/windSim_textBased).

447

448 **Author contributions**

449 Zeen Zhu implemented the method, performed the analysis, produced the figures, and wrote the
450 inertial draft of the manuscript. Pavlos Kollias supervised and provided advice and guidance on
451 all aspects of the analysis and contributed to the writing of the manuscript. Fan Yang advised on
452 results interpretation and manuscript editing. All authors read the manuscript draft and contributed
453 comments.

454



455 **Financial support**

456 Zeen Zhu's contribution are supported by Brookhaven National Laboratory via Laboratory
457 Directed Research and Development Grant LDRD 22-054. Pavlos Kollias and Fan Yang are
458 supported by the US Department of Energy (DOE) under contract DE-SC0012704.

459

460

461 **Reference**

- 462 Acquistapace, C., Löhnert, U., Maahn, M., and Kollias, P.: A New Criterion to Improve
463 Operational Drizzle Detection with Ground-Based Remote Sensing, *Journal of Atmospheric and*
464 *Oceanic Technology*, 36, 781-801, 2019.
- 465 Atlas, D., Srivastava, R., and Sekhon, R. S.: Doppler radar characteristics of precipitation at
466 vertical incidence, *Reviews of Geophysics*, 11, 1-35, 1973.
- 467 Borque, P., Luke, E., and Kollias, P.: On the unified estimation of turbulence eddy dissipation
468 rate using Doppler cloud radars and lidars, *Journal of Geophysical Research: Atmospheres*, 121,
469 5972-5989, 2016.
- 470 Capsoni, C., D'Amico, M., and Nebuloni, R.: A multiparameter polarimetric radar simulator,
471 *Journal of Atmospheric and Oceanic Technology*, 18, 1799-1809, 2001.
- 472 Deodatis, G.: Simulation of ergodic multivariate stochastic processes, *Journal of engineering*
473 *mechanics*, 122, 778-787, 1996.
- 474 Doviak: Doppler radar and weather observations, Courier Corporation, 2006.
- 475 Gossard, E. E.: Measuring drop-size distributions in clouds with a clear-air-sensing Doppler
476 radar, *Journal of Atmospheric and Oceanic Technology*, 5, 640-649, 1988.
- 477 Gossard, E. E., and Strauch, R. G.: Further guide for the retrieval of drosize distributions in
478 water clouds with a ground-based clear-air-sensing Doppler radar, *NASA STI/Recon Technical*
479 *Report N*, 90, 11911, 1989.
- 480 Hildebrand, P. H., and Sekhon, R.: Objective determination of the noise level in Doppler spectra,
481 *Journal of Applied Meteorology*, 13, 808-811, 1974.
- 482 Kalesse, H., Szyrmer, W., Kneifel, S., Kollias, P., and Luke, E.: Fingerprints of a riming event
483 on cloud radar Doppler spectra: observations and modeling, *Atmospheric Chemistry and Physics*
484 *(Online)*, 16, 2016.
- 485 Khvorostyanov, V. I., and Curry, J. A.: Fall velocities of hydrometeors in the atmosphere:
486 Refinements to a continuous analytical power law, *Journal of the atmospheric sciences*, 62,
487 4343-4357, 2005.
- 488 Kollias, Albrecht, B. A., Lhermitte, R., and Savtchenko, A.: Radar observations of updrafts,
489 downdrafts, and turbulence in fair-weather cumuli, *Journal of the atmospheric sciences*, 58,
490 1750-1766, 2001.
- 491 Kollias, Clothiaux, E. E., Albrecht, B. A., Miller, M. A., Moran, K. P., and Johnson, K. L.: The
492 atmospheric radiation measurement program cloud profiling radars: An evaluation of signal
493 processing and sampling strategies, *Journal of Atmospheric and Oceanic Technology*, 22, 930-
494 948, 10.1175/jtech1749.1, 2005.
- 495 Kollias, Clothiaux, E., Miller, M., Albrecht, B., Stephens, G., and Ackerman, T.: Millimeter-
496 wavelength radars: New frontier in atmospheric cloud and precipitation research, *Bulletin of the*
497 *American Meteorological Society*, 88, 1608-1624, 2007.



- 498 Kollias, Remillard, J., Luke, E., and Szyrmer, W.: Cloud radar Doppler spectra in drizzling
499 stratiform clouds: 1. Forward modeling and remote sensing applications, *Journal of Geophysical*
500 *Research-Atmospheres*, 116, 10.1029/2010jd015237, 2011a.
- 501 Kollias, Szyrmer, W., Remillard, J., and Luke, E.: Cloud radar Doppler spectra in drizzling
502 stratiform clouds: 2. Observations and microphysical modeling of drizzle evolution, *Journal of*
503 *Geophysical Research-Atmospheres*, 116, 10.1029/2010jd015238, 2011b.
- 504 Kollias, P., Albrecht, B. A., and Marks, F.: Why Mie? Accurate observations of vertical air
505 velocities and raindrops using a cloud radar, *Bulletin of the American Meteorological Society*,
506 83, 1471-1483, 10.1175/bams-83-10-1471, 2002.
- 507 Kollias, P., Clothiaux, E. E., Ackerman, T. P., Albrecht, B. A., Widener, K. B., Moran, K. P.,
508 Luke, E. P., Johnson, K. L., Bharadwaj, N., and Mead, J. B.: Development and applications of
509 ARM millimeter-wavelength cloud radars, *Meteorological Monographs*, 57, 17.11-17.19, 2016.
- 510 Lhermitte, R. M.: Centimeter & millimeter wavelength radars in meteorology, Lhermitte
511 Publications, 2002.
- 512 Li, H., and Moisseev, D.: Two layers of melting ice particles within a single radar bright band:
513 Interpretation and implications, *Geophysical Research Letters*, 47, e2020GL087499, 2020.
- 514 Luke, E. P., Kollias, P., Johnson, K. L., and Clothiaux, E. E.: A technique for the automatic
515 detection of insect clutter in cloud radar returns, *Journal of Atmospheric and Oceanic*
516 *Technology*, 25, 1498-1513, 10.1175/2007jtecha953.1, 2008.
- 517 Luke, E. P., Kollias, P., and Shupe, M. D.: Detection of supercooled liquid in mixed-phase
518 clouds using radar Doppler spectra, *Journal of Geophysical Research-Atmospheres*, 115,
519 10.1029/2009jd012884, 2010.
- 520 Luke, E. P., Yang, F., Kollias, P., Vogelmann, A. M., and Maahn, M.: New insights into ice
521 multiplication using remote-sensing observations of slightly supercooled mixed-phase clouds in
522 the Arctic, *Proceedings of the National Academy of Sciences*, 118, e2021387118, 2021.
- 523 Maahn, M., Loehnert, U., Kollias, P., Jackson, R. C., and McFarquhar, G. M.: Developing and
524 Evaluating Ice Cloud Parameterizations for Forward Modeling of Radar Moments Using in situ
525 Aircraft Observations, *Journal of Atmospheric and Oceanic Technology*, 32, 880-903,
526 10.1175/jtech-d-14-00112.1, 2015.
- 527 Marshall, J. S., and Palmer, W. M. K.: The distribution of raindrops with size, *Journal of*
528 *meteorology*, 5, 165-166, 1948.
- 529 Mech, M., Maahn, M., Kneifel, S., Ori, D., Orlandi, E., Kollias, P., Schemann, V., and Crewell,
530 S.: PAMTRA 1.0: the Passive and Active Microwave radiative TRAnsfer tool for simulating
531 radiometer and radar measurements of the cloudy atmosphere, *Geoscientific Model*
532 *Development*, 13, 4229-4251, 2020.
- 533 Moisseev, D. N., and Chandrasekar, V.: Polarimetric spectral filter for adaptive clutter and noise
534 suppression, *Journal of Atmospheric and Oceanic Technology*, 26, 215-228, 2009.
- 535 Mróz, K., Battaglia, A., Kneifel, S., von Terzi, L., Karrer, M., and Ori, D.: Linking rain into ice
536 microphysics across the melting layer in stratiform rain: a closure study, *Atmospheric*
537 *Measurement Techniques*, 14, 511-529, 2021.
- 538 Nijhuis, A. C. O., Yanovsky, F. J., Krasnov, O., Unal, C. M., Russchenberg, H. W., and
539 Yarovoy, A.: Assessment of the rain drop inertia effect for radar-based turbulence intensity
540 retrievals, *International Journal of Microwave and Wireless Technologies*, 8, 835, 2016.
- 541 Oue, M., Kollias, P., Ryzhkov, A., and Luke, E. P.: Toward exploring the synergy between cloud
542 radar polarimetry and Doppler spectral analysis in deep cold precipitating systems in the Arctic,
543 *Journal of Geophysical Research: Atmospheres*, 123, 2797-2815, 2018.



544 Oue, M., Tatarevic, A., Kollias, P., Wang, D., Yu, K., and Vogelmann, A.: The Cloud-resolving
545 model Radar SIMulator (CR-SIM) Version 3.3: description and applications of a virtual
546 observatory, *Geoscientific Model Development (Print)*, 13, 2020.
547 Silber, I., Jackson, R. C., Fridlind, A. M., Ackerman, A. S., Collis, S., Verlinde, J., and Ding, J.:
548 The Earth Model Column Collaboratory (EMC 2) v1. 1: an open-source ground-based lidar and
549 radar instrument simulator and subcolumn generator for large-scale models, *Geoscientific Model*
550 *Development*, 15, 901-927, 2022.
551 Wang, D., Bartholomew, M. J., Giangrande, S. E., and Hardin, J. C.: Analysis of Three Types of
552 Collocated Disdrometer Measurements at the ARM Southern Great Plains Observatory, Oak
553 Ridge National Lab.(ORNL), Oak Ridge, TN (United States). *Atmospheric ...*, 2021.
554 Williams: Vertical air motion retrieved from dual-frequency profiler observations, *Journal of*
555 *Atmospheric and Oceanic Technology*, 29, 1471-1480, 2012.
556 Williams, C. R., Maahn, M., Hardin, J. C., and de Boer, G.: Clutter mitigation, multiple peaks,
557 and high-order spectral moments in 35 GHz vertically pointing radar velocity spectra,
558 *Atmospheric Measurement Techniques*, 11, 4963-4980, 10.5194/amt-11-4963-2018, 2018.
559 Yanovsky, F.: Simulation study of 10 GHz radar backscattering from clouds, and solution of the
560 inverse problem of atmospheric turbulence measurements, *IEE Conference Publication*, 1996,
561 188-193,
562 Zhu, Z., Kollias, P., Yang, F., and Luke, E.: On the estimation of in-cloud vertical air motion
563 using radar Doppler spectra, *Geophysical Research Letters*, 48, e2020GL090682, 2021.
564 Zhu, Z., Kollias, P., Luke, E., and Yang, F.: New insights on the prevalence of drizzle in marine
565 stratocumulus clouds based on a machine learning algorithm applied to radar Doppler spectra,
566 *Atmospheric Chemistry and Physics*, 22, 7405-7416, 2022.
567
568
569